reduce the input reflection of a corrugated feed," *Bell Syst. Tech. J.* Feb. 1984.
[10] C. Dragone, "A rectangular horn of four corrugated plates," submitted to *IEEE Trans. Antennas Propagat.*
[11] C. Dragone, "High-frequency behavior of waveguides with finite surface impedances," *Bell Syst. Tech. J.*, vol. 60, no. 1, pp. 89–115, Jan. 1981.
[12] V. L. Rumsey, "Horn antennas with uniform power patterns around their axes," *IEEE Trans. Antennas Propagat.*, vol. AP-14, p. 656, Sept. 1966.
[13] R. B. Dydbal, L. Peters, and W. H. Peake, "Rectangular waveguide and impedance walls," *IEEE Trans. Microwave Theory Tech.*, vol. MTT-19, no. 1, pp. 2–9, Jan. 1971.

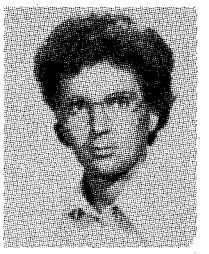

Corrado Dragone (SM'84) received the Laurea in electrical engineering from Padua University, Italy, in 1961 and the Libera Docenza from the Ministero della Pubblica Istruzione, Italy, in 1968.

Since joining Bell Laboratories in 1961, he has been engaged in experimental and theoretical work on microwave antennas and solid-state power sources. In 1974 and 1975, he taught a course on antennas and propagation at Padua University. He is currently concerned with problems involving electromagnetic wave propagation and microwave antennas for terrestrial radio systems and satellite communications.

High-Temperature Microwave Characterization of Dielectric Rods

JOSE C. ARANETA, MEMBER, IEEE, MORRIS E. BRODWIN, SENIOR MEMBER, IEEE, AND GREGORY A. KRIEGSMANN

Abstract—**A technique for the simultaneous heating and characterization of dielectric rods using a single microwave source is described. The rod is heated in a rectangular cavity excited by an iris. A variational model for the impedances of homogeneous rods used in the characterization procedure is discussed. It is accurate regardless of the diameter of the rod, even at resonance. Experimental results of β-Al_2O_3 are presented.**

I. Introduction

THE CHARACTERIZATION technique to be described is unique in allowing the simultaneous heating and characterization of a dielectric rod while using a single microwave generator. An earlier technique utilized two microwave sources [1].

The inherent speed of microwave heating can result in a significant amount of energy savings and greater throughput of heat-treated rods as compared to conventional heating.

In sintering ceramic rods, the speed of microwave heating makes it possible to discriminate against deleterious slow diffusion processes associated with grain growth [2], [3].

The technique is particularly suitable for processing high-technology ceramics such as β-Al_2O_3, a solid electrolyte used in high-energy density batteries. It can also be used to sinter and characterize high-permittivity ceramics as well as piezoelectric ceramics and ferrites.

Manuscript received November 22, 1983; revised April 19, 1984. This work was supported by the Army Research Office under Contract No. DAAG29-80-K-0031.

J. C. Araneta and M. E. Brodwin are with the Department of Electrical Engineering and Computer Science, Northwestern University, Evanston, IL 60201.

G. A. Kriegsmann is with the Department of Engineering Sciences and Applied Mathematics, Northwestern University, Evanston, IL 60201.

In situ characterization while sintering provides insight into sintering dynamics without the disadvantages of electrodes.

The applicator used to heat and characterize the rod is a rectangular cavity excited by an iris. The rod is mounted in the cavity parallel to the electric-field vector. The dielectric constant and electric conductivity of the rod are deduced by equating the measured admittance of the cavity with the inserted rod with the corresponding admittance derived from the equivalent-circuit representation.

An accurate equivalent circuit representation of the rod is therefore necessary. Marcuvitz [4] gave a variational model for the rod which is accurate only when the rod is very thin compared to the wavelength. It is also invalid near "resonance." Nielsen [5] described a numerical technique which eliminates the limitation on the diameter of the rod. Although Nielsen's method shows an improved representation near resonance, it too suffers a similar deficiency. These models are valid only when the rod is homogeneous, i.e., the electric conductivity and dielectric constant are uniform throughout the rod.

An improved variational model is presented in Section II. It is derived from the same variational formulation attributed to Schwinger [6] that Marcuvitz used. The improved variational model has no restriction on the rod diameter and also yields accurate results in the region of resonance. As compared to the numerical technique of Nielsen [5], the improved variational model is also easier to implement and converges more rapidly. The improvement was realized by using higher order approximations to the variational solution of Schwinger.

The characterization procedure, Section III, involves the equating of the measured and theoretical admittances. This

0018-9480/84/1000-1328$01.00 ©1984 IEEE

gives rise to a transcendental equation whose roots yield the complex dielectric constant. A modified bisection method [7] is used to determine these roots.

Section IV describes the experimental techniques used to determine the electric conductivity and dielectric constant of β-Al_2O_3 as a function of temperature. The temperature of the rod is maintained at a desired value by employing a negative-feedback control scheme.

The electric conductivity of β-Al_2O_3 increased as temperature increased. On the other hand, its dielectric constant decreased as temperature increased. Similar results have been presented earlier [8].

II. Variational Model for Homogeneous Rods

The accuracy of the characterization procedure is greatly dependent on the accuracy of the equivalent circuit model used to represent the rod. A model based on Schwinger's variational formulation [6] for the impedances of the T-equivalent circuit of the rod is used in the characterization procedure that will be described. A model cited by Marcuvitz [4] is actually an approximation to the results that come after the implementation of Schwinger's variational formulation. In any case, the characterization procedure requires a model for a circular rod mounted parallel to the electric field of the TE_{10} mode.

Marcuvitz's approximation is accurate only when the diameter of the rod is small relative to the wavelength and when the value of the dielectric constant of the rod is not near a "resonance" condition of the model.

However, the limitations imposed on the application of Marcuvitz's approximation can be removed by an appropriate use of higher order approximations to the variational solution.

Using Schwinger's notation, the equivalent circuit for the rod is shown in Fig. 1, where P denotes the reference plane on the waveguide passing through the axis of the rod, and the impedances are normalized by Z_0.

The expressions for the impedances [6] when an $\exp(j\omega t)$ time dependence is used are

$$j(Z_{11}+Z_{12})\frac{(\epsilon_r^*-1)k^2}{\kappa a}=\frac{\int\varphi_e^2(x,z)\,dS-(\epsilon_r^*-1)k^2\int\int\varphi_e(x,z)G'(x,z|x',z')\varphi_e(x',z')\,dS\,dS'}{\left(\int\varphi_e\psi_e\,dS\right)^2} \tag{1}$$

$$\frac{j(\epsilon_r^*-1)k^2}{\kappa a(Z_{11}-Z_{12})}=\frac{\int\varphi_0^2(x,z)\,dS-(\epsilon_r^*-1)k^2\int\int\varphi_0(x,z)G'(x,z|x',z')\varphi_0(x',z')\,dS\,dS'}{\left(\int\varphi_0\psi_0\,dS\right)^2} \tag{2}$$

where the integration is over the cross section of the rod and

$$G'(x,z|x',z')=-\frac{1}{\kappa a}\sin\frac{\pi x}{a}\sin\frac{\pi x'}{a}\sin\kappa|z-z'|+\frac{1}{a}\sum_{n=2}^{\infty}\frac{1}{|\kappa_n|}\sin\frac{n\pi x}{a}\sin\frac{n\pi x'}{a}e^{-|\kappa_n(z-z')|} \tag{3}$$

is the real part of the Green's function for the infinite rectangular waveguide, and where "k" is the propagation constant in free-space, ϵ_r^* is the complex dielectric constant of the rod, and $\kappa_n^2=k^2-(n\pi/a)^2$ is the propagation constant of the TE_{no} mode in the waveguide. Note that $\kappa_1=\kappa=2\pi/\lambda_g$ where λ_g is the wavelength in the waveguide.

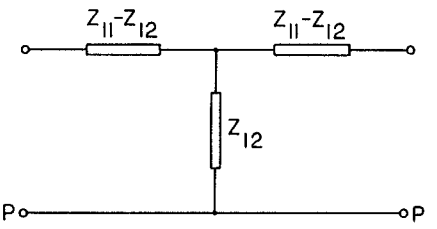

Fig. 1. T-equivalent circuit.

The functions ψ_e and ψ_o are the even and odd TE_{10} mode electric-field intensities, while the functions φ_e and φ_o are the even and odd solutions of the wave equation

$$(\nabla^2+\epsilon_r^*k^2)\varphi=0. \tag{4}$$

The even and odd functional symmetry is about the reference plane P.

Using the coordinates shown in Fig. 2, the solution to (4), given in [6] when $\epsilon_r^*(x,z)$ is constant, simplifies to

$$\varphi_e(r,\theta)=\sum_{m=0}^{\infty}A_{2m}\cos 2m\theta J_{2m}\left(\sqrt{\epsilon_r^*}kr\right) \tag{5}$$

$$\varphi_o(r,\theta)=\sum_{m=0}^{\infty}B_{2m+1}\cos(2m+1)\theta J_{2m+1}\left(\sqrt{\epsilon_r^*}kr\right) \tag{6}$$

due to symmetry about the $x=a/2$ plane when the rod is at the middle of the waveguide. The dimension of the broad side of the waveguide is denoted by "a" and the radius of the rod is "R." The axis of the rod is the line $(a/2, y, 0)$.

A first approximation to (5) and (6) utilizes only the first terms. Calling this the 1×1 approximation, the expressions to be used in (1) and (2) are

$$\varphi_e(r,\theta)\simeq A_0J_0\left(\sqrt{\epsilon_r^*}kr\right) \tag{7}$$

$$\varphi_o(r,\theta)\simeq B_1\cos\theta J_1\left(\sqrt{\epsilon_r^*}kr\right). \tag{8}$$

Using (7) and (3) in (1) results in [7]

$$Z_{11}+Z_{12}=j\kappa a\left\{\frac{1}{\pi}\sum_{3,\mathrm{ODD}}^{\infty}\left[n^2-\left(\frac{ka}{\pi}\right)^2\right]^{-1/2}-\frac{1}{n}+\frac{1}{2\pi}\log_e\left(\frac{kaC}{\pi}\right)-\frac{1}{\pi}+\frac{1}{4}\left[\frac{\beta J_1(\beta)Y_0(\alpha)-\alpha J_0(\beta)Y_1(\alpha)}{\alpha J_0(\beta)J_1(\alpha)-\beta J_1(\beta)J_0(\alpha)}\right]\right\} \tag{9}$$

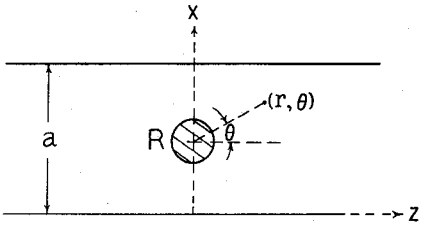

Fig. 2. Rod coordinates relative to the waveguide.

where $\alpha = kR$, $\beta^2 = \epsilon_r^* \alpha^2$, and $\log_e C = 0.57721566490$.

Using (3) and (8) in (2) with the same location of the rod axis results in [7]

$$-j\frac{(\kappa R^2/a)}{(Z_{11}-Z_{12})} = \alpha^2 \lim_{\substack{r\to 0\\ r'\to 0}} \left(\frac{1}{k}\right)^2 \frac{\partial^2 \Gamma'}{\partial z \partial z'} + \frac{\alpha^2}{8}\left[\frac{\beta J_0(\beta)Y_1(\alpha)-\alpha J_1(\beta)Y_0(\alpha)}{\alpha J_1(\beta)J_0(\alpha)-\beta J_0(\beta)J_1(\alpha)}\right] \quad (10)$$

where

$$\Gamma'(x,z|x',z') = G'(x,z|x',z') + \frac{1}{4}Y_0(k|r-r'|) \quad (11)$$

is the difference between the real parts of the Green's function of the infinite rectangular waveguide and the free-space Green's function. The limit of the first term on the right-hand side is [7]

$$\lim_{\substack{r\to 0\\ r'\to 0}} \left(\frac{1}{k}\right)^2 \frac{\partial^2 \Gamma'}{\partial z \partial z'} = \frac{\pi}{(ka)^2}\left\{\sum_{3,\mathrm{ODD}}^{\infty}\left[n - \sqrt{n^2-\left(\frac{ka}{\pi}\right)^2} - \frac{1}{2n}\left(\frac{ka}{\pi}\right)^2\right] + \frac{7}{8} - \frac{1}{2}\left\{\left(\frac{ka}{\pi}\right)^2 + \left(\frac{ka}{2\pi}\right)^2 \log_e\left(\frac{2ka}{\pi}\right)\right\}\right. . \quad (12)$$

We shall now show that applying the condition $\alpha \ll 1$ to the 1×1 approximation leads to the Marcuvitz equations. The simplification of $\beta J_1(\beta)Y_0(\alpha) - \alpha J_0(\beta)Y_1(\alpha)$ in (9) when $\alpha \ll 1$ gives

$$Z_{11}+Z_{12} \cong j\left(\frac{a}{\lambda_g}\right)\left\{2\sum_{3,\mathrm{ODD}}^{\infty}\left[n^2-\left(\frac{ka}{\pi}\right)^2\right]^{-1/2} - \frac{1}{n} + \log_e\left(\frac{2a}{\pi R}\right) - 2 - \left(\frac{\alpha}{2}\right)^2 + \frac{J_0(\beta)}{J_0(\alpha)} \cdot \frac{1}{[\alpha J_0(\beta)J_1(\alpha)-\beta J_1(\beta)J_0(\alpha)]}\right\} \quad (13)$$

while the same condition applied to $\beta J_o(\beta)Y_1(\alpha) - \alpha J_1(\beta)Y_o(\alpha)$ in (10) results in the dropping of the first term on the right-hand side of (10) and the simplification of the second. The result is

$$Z_{11}-Z_{12} \cong \frac{-j\left(\frac{a}{\lambda_g}\right)\left(\frac{2\pi R}{a}\right)^2}{1-\frac{1}{2}\alpha^2\frac{J_1(\beta)}{J_1(\alpha)}\frac{1}{[\alpha J_1(\beta)J_0(\alpha)-\beta J_0(\beta)J_1(\alpha)]}} . \quad (14)$$

The simplification can be carried out because, for most cases, the value of β does not make the second term smaller than the first. For this situation, the magnitude of the first term relative to the second is of order α^2.

Equations (13) and (14) are the Marcuvitz approximations. As Marcuvitz stated, "They are within a few percent error when $R/a < 0.075$ and $0.2 < x_o/a < 0.8$." The second restriction is dictated by the fact that (7) and (8) are only true when the rod is at the middle of the waveguide. Note that x_o denotes the location of the axis of the rod when it is off centered.

A resonant condition is one that makes one of the branches of the T-equivalent circuit either zero or infinite. The values of the parameters at which resonance occurs depend upon which approximation is being used.

For instance, the value of β that makes $Z_{11}-Z_{12}$ infinite satisfies

$$J_1(\alpha)[\alpha J_1(\beta)J_0(\alpha)-\beta J_0(\beta)J_1(\alpha)] - \frac{1}{2}\alpha^2 J_1(\beta) = 0 \quad (15)$$

when the Marcuvitz approximation (14) is used while it satisfies

$$\lim_{\substack{r\to 0\\ r'\to 0}} \left(\frac{1}{k}\right)^2 \frac{\partial^2 \Gamma'}{\partial z \partial z'} + \frac{1}{8}\left[\frac{\beta J_0(\beta)Y_1(\alpha)-\alpha J_1(\beta)Y_0(\alpha)}{\alpha J_1(\beta)J_0(\alpha)-\beta J_0(\beta)J_1(\alpha)}\right] = 0 \quad (16)$$

when the 1×1 approximation (10) is used. The value of β at "resonance" is different in the two cases.

When the value of β is close to the root of (15), the Marcuvitz approximation becomes inaccurate. The first term on the right-hand side of (10) dominates and the 1×1 approximation of (9) and (10) should be used. If β is close to the root of (16), the more accurate 2×2 approximation may be used.

The 2×2 approximation is derived by using the first two terms of (5) and (6)

$$\varphi_e(r,\theta) \simeq A_0 J_0\left(\sqrt{\epsilon_r^*}\,kr\right) + A_2 \cos 2\theta J_2\left(\sqrt{\epsilon_r^*}\,kr\right) \quad (17)$$

$$\varphi_o(r,\theta) \simeq B_1 \cos\theta J_1\left(\sqrt{\epsilon_r^*}\,kr\right) + B_3 \cos 3\theta J_3\left(\sqrt{\epsilon_r^*}\,kr\right). \quad (18)$$

Using (17) in (1) and (18) in (2) gives [7]

$$\frac{1}{Z_{11}+Z_{12}} = -j\frac{(\epsilon_r^*-1)k^2}{\kappa a} \cdot \left[\frac{C_0^2 - C_0C_2(D_{02}+D_{20})/D_{22} + C_2^2 D_{00}/D_{22}}{D_{00}-(D_{02}D_{20}/D_{22})}\right] \quad (19)$$

$$Z_{11}-Z_{12} = -j\frac{(\epsilon_r^*-1)k^2}{\kappa a} \cdot \left[\frac{C_1^2 - C_1C_3(D_{13}+D_{31})/D_{33} + C_3^2 D_{11}/D_{33}}{D_{11}-(D_{13}D_{31}/D_{33})}\right] \quad (20)$$

where the detailed expressions for the C_i's and D_{ij}'s are listed in the Appendix.

TABLE I
SOME VALUES OF ϵ_r THAT SATISFY (25)–(27)

α	Eq. (27)	Eq. (26)	Eq. (25)
0.1	574	1,469	2,637
	3,042	4,923	7,085
0.2	141	368	659
	758	1,231	1,771

When

$$|C_0^2| \gg |-C_0C_2(D_{02}+D_{20})/D_{22}+C_2^2D_{00}/D_{22}| \quad (21a)$$

$$|D_{00}| \gg |D_{02}D_{20}/D_{22}| \quad (21b)$$

are satisfied, (19) reduces to the 1×1 approximation for $Z_{11}+Z_{12}$, and when

$$|C_1^2| \gg |-C_1C_3(D_{13}+D_{31})/D_{33}+C_3^2D_{11}/D_{33}| \quad (22a)$$

$$|D_{11}| \gg |D_{13}D_{31}/D_{33}| \quad (22b)$$

are satisfied, (20) reduces to the 1×1 approximation for $Z_{11}-Z_{12}$.

There are four types of resonance: 1) $Z_{11}-Z_{12}$ is zero, 2) $Z_{11}-Z_{12}$ is infinite, 3) $Z_{11}+Z_{12}$ is zero, and 4) $Z_{11}+Z_{12}$ is infinite. The corresponding conditions for the 1×1 approximation are

$$C_1=0 \qquad D_{11}=0 \quad (23a,b)$$

$$C_0=0 \qquad D_{00}=0. \quad (24a,b)$$

Equation (23a) is satisfied when

$$\alpha J_1(\beta)J_0(\alpha)-\beta J_0(\beta)J_1(\alpha)=0 \quad (25)$$

while (24a) is satisfied when

$$\alpha J_0(\beta)J_1(\alpha)-\beta J_1(\beta)J_0(\alpha)=0. \quad (26)$$

Both the 1×1 and Marcuvitz approximations will give a zero value for $Z_{11}-Z_{12}$ when (25) is satisfied. Both approximations will give an infinite value for $Z_{11}+Z_{12}$ when (26) is satisfied. The 1×1 approximation will give a zero value for $Z_{11}+Z_{12}$ when D_{00} is zero and an infinite value for $Z_{11}-Z_{12}$ when D_{11} is zero.

When (23) and (24) are satisfied, the 2×2 approximation must be used in place of the 1×1 approximation.

Note that the resonance condition for the Marcuvitz approximation expressed by (15) can be replaced with the same order of accuracy by

$$\alpha J_1(\beta)Y_0(\alpha)-\beta J_0(\beta)Y_1(\alpha)=0. \quad (27)$$

For a given rod diameter, there is an infinite number of ϵ_r^* that satisfies (25), (26), and (27). Since $\epsilon_r^*=(\beta/\alpha)^2$, smaller rods have larger values of ϵ_r^* at resonance.

Equations (23) and (24) are useful in choosing rod diameters which avoid resonances and therefore avoid the use of the more complicated 2×2 approximation.

The first few values of ϵ_r^* that satisfy (25)–(27), when ϵ_r^* is real, are shown in Table I.

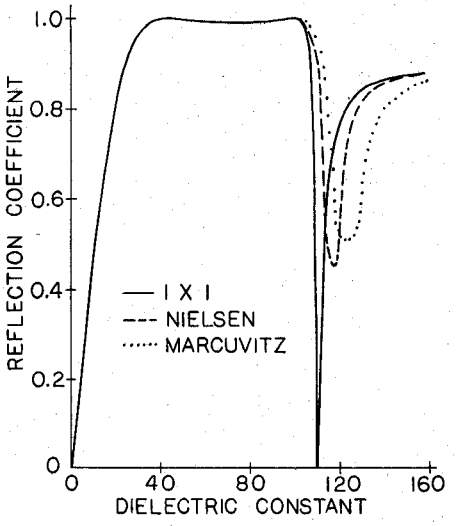

Fig. 3. Magnitude of reflection coefficient as a function of dielectric constant.

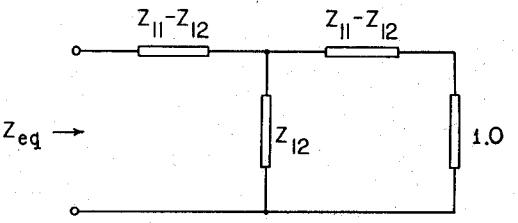

Fig. 4. Equivalent circuit of the rod in an infinite waveguide.

To illustrate the relative accuracy of the 1×1 approximation, let us review the example used by Nielsen [5]. He compared the results of his numerical technique for the reflection coefficient of the rod with those derived using the Marcuvitz approximation. Fig. 3 of [5] is reproduced in Fig. 3 as the dashed and dotted curves. The relevant parameters are $R/a=0.05$ and $\alpha=0.2243$. This figure shows a dip in $|\rho|$ in the range $115<\epsilon_r<120$. Marcuvitz's result exhibits a minimum of $|\rho|\approx0.51$ at $\epsilon_r\approx120$, while Nielsen's result shows a minimum of $|\rho|\approx0.45$ at $\epsilon_r\approx115$.

The minima in $|\rho|$ shown in Fig. 3 occurs in the vicinity of the value of ϵ_r that makes $Z_{11}-Z_{12}$ infinite. This "resonant" value of ϵ_r satisfies (15) when the Marcuvitz approximation is used, and it satisfies (16) when the 1×1 approximation is used. Note that (16) is the same as the resonant condition $D_{11}=0$ expressed by (23b). A value of ϵ_r that satisfies (16) is 108.9.

We shall now determine $|\rho|$ using the 1×1 and 2×2 approximations and compare the result with Nielsen's and Marcuvitz's.

The normalized equivalent circuit of the rod in an infinite waveguide or a finite waveguide terminated by Z_o is shown in Fig. 4. After finding the equivalent impedance Z_{eq}, it can be shown that

$$|\rho|=\left|\frac{(Z_{11}+Z_{12})-(Z_{11}-Z_{12})^{-1}}{[1-(Z_{11}+Z_{12})][1+(Z_{11}-Z_{12})^{-1}]}\right|. \quad (28)$$

The 1×1 approximation was used to calculate $Z_{11}+Z_{12}$ since (21) was satisfied in the range $\epsilon_r<200$. However, both the 1×1 and 2×2 approximations were used to

calculate $Z_{11}-Z_{12}$ [7]. The 2×2 approximation was also used to calculate $Z_{11}-Z_{12}$, particularly at $\epsilon_r=108.9$, because the 1×1 approximation is resonant there. However, the results for $Z_{11}-Z_{12}$ using the 1×1 approximation agree to within four significant figures with the results derived from the 2×2 approximation and this is the case even at $\epsilon_r=108.9$.

Fig. 3 shows the results derived from (28) and the 1×1 approximation as a solid curve. The results of the 2×2 approximation is a curve that coincides with the solid curve. This means that the solid curve also represents the convergent variational solution. It shows a dip in $|\rho|$ at $\epsilon_r=110.0$ and the value of $|\rho|$ there is zero. Note that resonance for the 1×1 approximation occurs at $\epsilon_r=108.9$, and it is not the same value of ϵ_r at which minimum $|\rho|$ occurs.

The expression for φ that Nielsen used is the same as (7) and (8) combined. For the example reviewed above, he utilized ten terms in his calculations, while the 1×1 approximation used only two. Furthermore, the 1×1 and the 2×2 approximations, to the variational solution for $|\rho|$, agree. These facts suggest that the variational solution converges to the exact answer more rapidly than the Nielsen numerical technique. In addition, they suggest that the variational solution is computationally more efficient.

The details of the $n\times n$ approximation to the variational solution are given in [6], [7].

III. Characterization Procedure

The equivalent circuit of the rectangular cavity applicator loaded with the rod is shown in Fig. 5. The rod is represented by its T-equivalent circuit, while the iris and short circuit are represented by equivalent shunt admittances y_i and y_s, respectively. The distance between the iris and the axis of the rod is denoted by l_1, while the distance between the plane of the short circuit and the axis of the rod is denoted by l_2.

The electric conductivity σ and the dielectric constant ϵ_r of the rod are determined by equating the equivalent admittance y_c of the circuit shown in Fig. 5 to the measured admittance y_m.

The admittance y_m is measured by using a standing-wave machine. A convenient reference plane for y_m is the plane of the iris. Hence

$$y_m=\frac{S-j\tan\kappa d}{1-jS\tan\kappa d} \tag{29}$$

where d is the distance of a standing-wave minimum from the reference plane and S is the standing-wave ratio.

Before the equivalent admittance of the circuit y_c can be calculated, the following quantities must be measured: rod diameter, admittances y_s and y_i, and the distances l_1 and l_2.

The values of $Z_{11}+Z_{12}$ and $Z_{11}-Z_{12}$ are calculated to the desired degree of accuracy by using the appropriate approximation to the variational model.

The equivalent circuit admittance may be expressed as

$$y_c=y_i+\frac{y_T+j\tan\kappa l_1}{1+jy_T\tan\kappa l_1} \tag{30}$$

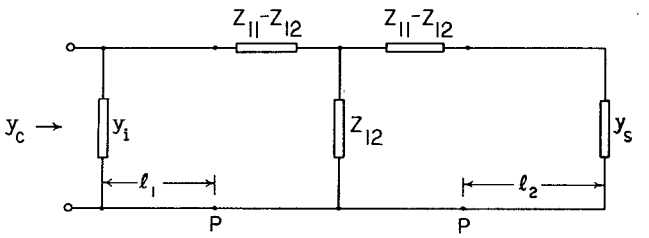

Fig. 5. Equivalent circuit of the cavity and rod.

where

$$y_T=\frac{Z_{11}+z_3}{(Z_{11}-Z_{12})(Z_{11}+Z_{12})+Z_{11}z_3} \tag{31}$$

and the equivalent impedance of the short circuit evaluated at the axis of the rod denoted by z_3 is

$$z_3=\frac{1+jy_s\tan\kappa l_2}{y_s+j\tan\kappa l_2}. \tag{32}$$

If the distance l_1 is an odd-multiple of a quarter of the wavelength inside the waveguide, (30) simplifies to

$$y_c\equiv y_i+y_T^{-1}. \tag{33}$$

The only factor in y_c that can be treated as a variable while characterizing the rod is β. The value of β that makes $y_c=y_m$ determines the measured values of σ and ϵ_r. Denoting this by β_o, the electric conductivity and dielectric constant are determined from

$$\epsilon_r-j\frac{\sigma}{\omega\epsilon_o}=\left(\frac{\beta_o}{\alpha}\right)^2. \tag{34}$$

The complex root β_o is found by setting

$$F(\beta)\equiv\mathrm{Re}(y_c-y_m)=0 \tag{35a}$$

$$G(\beta)\equiv\mathrm{Im}(y_c-y_m)=0. \tag{35b}$$

The intersection of the two curves defined by (35) on the complex β plane is the complex root β_o.

We shall now describe the numerical technique used to find the complex root β_o. The function y_c-y_m is evaluated over a radial range of β. The magnitude of β is varied but its phase angle is fixed. The bisection method is used twice; once to find the roots of $G(\beta)$. In looking for the roots of $F(\beta)$ and secondly to find the roots of $F(\beta)$, the real part of the numerical value of y_c-y_m is monitored. Similarly, the imaginary part of the numerical value of y_c-y_m is monitored in looking for the roots of $G(\beta)$. If no root of $F(\beta)$ is equal to a root of $G(\beta)$, the process is repeated at another phase angle of β. The change in phase angle is continued in the direction that eventually makes a root of $F(\beta)$ coincident with a root of $G(\beta)$. When this happens, the common root is β_o.

In general, more than one root will be found for each of the functions expressed in (35). However, the experimental results discussed in the next section give a unique value of β_o.

The bisection method can only detect the presence of an odd number of roots in a given span of $|\beta|$. If an even number of roots exist, the method will not yield even a single root. However, this shortcoming can be easily remedied by specifying a shorter search span for $|\beta|$.

If ϵ_r is positive, (34) suggests that realistic values of β_o are confined to phase-angle ranges between 0 and $-\pi/4$, as well as between $3\pi/4$ and π. If negative ϵ_r are included, the feasible ranges expand to the whole second and fourth quadrants, respectively.

It is found by actual numerical calculation that a given value of σ and ϵ_r corresponds to two values of β_o, one in the feasible range of the second quadrant and the other in the feasible range of the fourth quadrant. This is because two values of β with the same magnitude and differing in phase angle by 180° give the same value of σ and ϵ_r, as can be seen in (34).

The values of β in the first and third quadrants of the complex β plane correspond to a negative electric conductivity. Whenever roots are found in these quadrants, they are clearly spurious. Hence, the search for β_o was limited to the feasible ranges of the second and fourth quadrants.

IV. High-Temperature Results for β-Al_2O_3

The experimental system used to measure the electric conductivity σ and dielectric constant ϵ_r of β-Al_2O_3 is shown in Fig. 6.

An important innovation incorporated into the system is the simultaneous heating and characterization of the rod with a single microwave generator. The microwave source used in the experiments was a Raytheon PGM-100. It has a maximum output of around 800 W and can be varied by varying the control current of a saturable-core reactor, which in turn regulates the anode current of the magnetron. It operates at 2.45 GHz.

The circulator diverts the power reflected from the applicator to the calorimeter where it is completely absorbed. In effect, the microwave generator, circulator, and calorimeter act as a source of internal impedance Z_o. Furthermore, the impedance presented to the generator is also Z_o. The interaction between the microwave generator and the applicator is thereby avoided, making it possible for the generator to maintain constant output power, regardless of the conditions of the applicator.

The applicator is a rectangular cavity which is used to measure the σ and ϵ_r of the rod and also heat it to the desired temperature [7]. The required amount of power from the microwave source to maintain a given temperature is minimized by "tuning" the cavity. This is achieved by adjusting the short circuit to the correct position and the iris to the correct size.

An automatic feedback control system is used to maintain the temperature of the rod at a desired value. It is actually the surface temperature of a small portion of the surface of the rod which is measured by the pyrometer and maintained constant. An adjustable voltage reference and a voltage-to-current converter completes the feedback loop via the control winding of the saturable-core reactor inside the microwave generator. Surface temperature is maintained by an automatic adjustment of the power output of the microwave generator.

The variation of the dielectric constant and electric conductivity of the rod with temperature is determined by repeating the characterization procedure at each temperature setting. Measurements of the standing wave are only made after a sufficiently long waiting period, e.g., 10 min, to ensure that steady-state conditions exist.

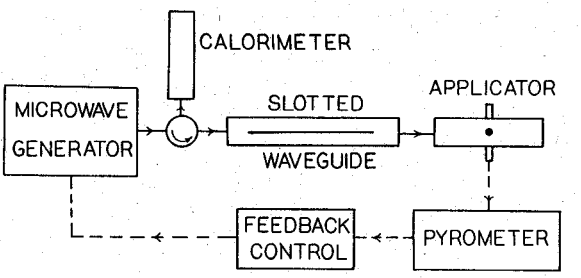

Fig. 6. The experimental system.

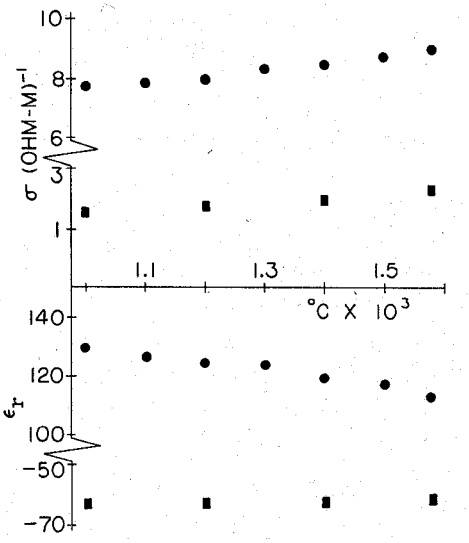

Fig. 7. Electric conductivity and dielectric constant of β-Al_2O_3 as a function of temperature. ●|×| and ■ Marcuvitz.

Consistent with the assumption of the variational model presented in Section II, only those rods that exhibit a uniform temperature profile can be characterized accurately. This is because a nonuniform temperature profile implies a nonuniform value of σ and ϵ_r. The measured results do not account for nonuniformities in σ and ϵ_r and therefore should be viewed as effective values.

Fig. 7 is a plot of electric conductivity σ and dielectric constant ϵ_r as a function of surface temperature of β-Al_2O_3.

The results shown in Fig. 7 were taken with the short-circuit position fixed throughout the experiment and no iris was used. The short circuit was maintained at $l_2 = 0.875\lambda_g$. These conditions were near the optimum settings for minimum power output to maintain constant temperature.

In addition, the rods were presintered by microwave heating, cooled to room temperature, and then characterized at the temperatures shown in the figure.

The diameter of the β-Al_2O_3 rod was equivalent to $\alpha = 0.1142$. This value of α suggests that the 1×1 approximation is sufficiently accurate. For comparison, the resulting values of σ and ϵ_r obtained by using the Marcuvitz approximation are also shown in Fig. 7. The results exhibit a dramatic discrepancy between the two approximations. The Marcuvitz electric conductivity is around 75 percent lower than those obtained with the 1×1

approximation. Moreover, the Marcuvitz dielectric constant is negative, while the dielectric constant obtained with the 1×1 approximation is positive. The values of the roots β_o given by the 1×1 approximation were relatively constant over the temperature range. These roots yield, however, a near resonance in the Marcuvitz approximation, i.e., the first term on the right-hand side of (10) is actually larger than the second. This contradicts the assumption used in deriving the Marcuvitz approximation.

The 1×1 results indicate an increasing conductivity and a decreasing dielectric constant as temperature increases from 1000 to 1580°C. A 13-percent change in both the values of σ and ϵ_r occurred between the two temperature extremes.

The constraints expressed by (21) and (22) were satisfied. Therefore, the use of the 2×2 approximation was unnecessary.

The above experiments were done with the rod exposed to the atmosphere. In addition, the upper half of the rod was at a slightly higher temperature due to convection since the rod was vertically oriented.

The characterization procedure was verified by measurements with distilled water at low power.

Appendix

The detailed expressions for the C_i's and the D_{ij}'s are

$$C_0 = \frac{-Q_0}{(\epsilon_r^*-1)k\alpha}$$

$$C_1 = \frac{-Q_1(\kappa/k)}{(\epsilon_r^*-1)k\alpha}$$

$$C_2 = \frac{Q_2}{(\epsilon_r^*-1)k\alpha}\left[1-2\left(\frac{\pi}{ka}\right)^2\right]$$

$$C_3 = \frac{Q_3(\kappa/k)}{(\epsilon_r^*-1)k\alpha}\left[1-4\left(\frac{\pi}{ka}\right)^2\right]$$

where $Q_n = \beta J_n(\alpha)J_{n-1}(\beta) - \alpha J_{n-1}(\alpha)J_n(\beta)$ for $n = 0,1,2,3$. The D_{ij}'s are given by

$$D_{00} = -(\epsilon_r^*-1)^{-1}\alpha^{-2}\left\{Q_0^2\Gamma'(0,0) + \frac{1}{4}Q_0[\beta Y_0(\alpha)J_1(\beta)-\alpha Y_1(\alpha)J_0(\beta)]\right\}$$

$$D_{11} = -(\epsilon_r^*-1)^{-1}\alpha^{-2}\left\{\left(\frac{Q_1}{k}\right)^2\Gamma'_{zz'}(0,0) - \frac{1}{8}Q_1[\beta Y_1(\alpha)J_0(\beta)-\alpha Y_0(\alpha)J_1(\beta)]\right\}$$

$$D_{22} = -(\epsilon_r^*-1)^{-1}\alpha^{-2}\left\{Q_2^2\left[\Gamma'(0,0)+\left(\frac{2}{k}\right)^2\Gamma'_{xx}(0,0) + \left(\frac{4}{k^4}\right)\Gamma'_{xxx'x'}(0,0)\right] - \frac{1}{8}Q_2[\beta Y_2(\alpha)J_1(\beta)-\alpha Y_1(\alpha)J_2(\beta)]\right\}$$

$$D_{33} = -(\epsilon_r^*-1)^{-1}\alpha^{-2}\left\{\left(\frac{Q_3}{k}\right)^2\left[\Gamma'_{zz'}(0,0)+\frac{8}{k^2}\Gamma'_{z'zxx}(0,0) + \left(\frac{2}{k}\right)^4\Gamma'_{z'zx^4}(0,0)\right] - \frac{1}{8}Q_3[\beta Y_3(\alpha)J_2(\beta)-\alpha Y_2(\alpha)J_3(\beta)]\right\}$$

$$D_{02} = D_{20} = \frac{-Q_0Q_2}{(\epsilon_r^*-1)\alpha^2}\left[\Gamma'(0,0)+\left(\frac{2}{k^2}\right)\Gamma'_{xx}(0,0)\right]$$

$$D_{13} = D_{31} = \frac{Q_1Q_3}{(\epsilon_r^*-1)\alpha^2k^2}\left[\Gamma_{zz'}(0,0)+\left(\frac{2}{k}\right)^2\Gamma'_{z'zxx}\right]$$

where

$$\pi\Gamma'(0,0) = \frac{1}{2}\log_e(cw) - 1 + \sum_{n=3,\text{ODD}}(n^2-w^2)^{-1/2} - n^{-1}$$

$$\left(\frac{\pi}{k^2}\right)\Gamma'_{z'z}(0,0) = w^{-2}\left\{\frac{7}{8}+\left(\frac{w}{2}\right)^2[\log_e(2w)-2] + \sum_{n=3,\text{ODD}} n-\sqrt{n^2-w^2}-\frac{w^2}{2n}\right\}$$

$$\left(\frac{\pi}{k^2}\right)\Gamma'_{xx}(0,0) = w^{-2}\left\{\frac{7}{8}-\left(\frac{w}{2}\right)^2[\log_e(2w)-2] + \sum_{n=3,\text{ODD}} n-n^2(n^2-w^2)^{-1/2}+\frac{w^2}{2n}\right\}$$

$$\left(\frac{\pi}{k^4}\right)\Gamma'_{x'x'xx}(0,0) = w^{-4}\left\{\frac{7w^2}{16}+\frac{3w^4}{16}(\log_e 2-2)-\frac{17}{16} + \sum_{n=3,\text{ODD}} n^4(n^2-w^2)^{-1/2} - n^3+\left(\frac{n}{2}\right)w^2-\frac{3w^4}{8n}\right\}$$

$$\left(\frac{\pi}{k^4}\right)\Gamma'_{z'zxx}(0,0) = w^{-4}\left\{\frac{7w^2}{16}+\frac{w^4}{16}(\log_e 2-2)-\frac{17}{16} + \sum_{n=3,\text{ODD}} n^2\sqrt{n^2-w^2} - n^3+\frac{nw^2}{2}+\frac{w^4}{8n}\right\}$$

$$\left(\frac{\pi}{k^6}\right)\Gamma'_{z'zx^4}(0,0) = w^{-6}\left\{\frac{25}{32}-\frac{17}{32}w^2+\frac{7w^4}{64} + 2\left(\frac{w}{2}\right)^6(2-\log_e 2) + \sum_{n=3,\text{ODD}} n^5-n^4\sqrt{n^2-w^2}-\frac{n^3w^2}{2} - \frac{nw^4}{8}-\frac{3w^6}{48n}\right\}$$

$$w = \frac{ka}{\pi}.$$

REFERENCES

[1] D. Couderc, M. Giroux, and R. G. Bosisio, "Dynamic high temperature complex permittivity measurements on samples heated via microwave absorption," *J. Microwave Power*, vol. 8, no. 1, pp. 69–82, 1973.

[2] A. J. Berteaud and J. C. Badot, "High temperature microwave heating in refractory materials," *J. Microwave Power*, vol. 11, no. 4, pp. 315–320, 1976.

[3] Ph. Colomban and J. C. Badot, "Elaboration de ceramiques superconductrices anisotropes ($Na^{+}\beta$-N_2O_3) par chauffage microondes," *Mat. Res. Bul.*, vol. 13, pp. 135–139, 1978.

[4] N. Marcuvitz, *Waveguide Handbook*. New York: McGraw-Hill, 1951, pp. 257–271.

[5] Erik D. Nielsen, "Scattering by a cylindrical post of complex permittivity in a waveguide," *IEEE Trans. Microwave Theory Tech.*, vol. MTT-17, pp. 148–153, Mar. 1969.

[6] Julian Schwinger, *Discontinuities in Waveguides: Notes on Lectures by Julian Schwinger*. New York: Gordon and Breach, 1968, Chapter II.

[7] Jose C. Araneta, "High temperature microwave heating and characterization of dielectric rods," Ph.D. dissertation, Northwestern University, Evanston, IL, 1984.

[8] A. S. Barker, J. A. Ditzenberger, and J. P. Remeika, "Lattice vibrations and ion transport spectra in β-alumina. II Microwave spectra," *Phys. Rev. B.*, vol. 14(10), pp. 4254–4265, Nov. 15, 1976.

Jose C. Araneta (S'81–M'83) received the B.S. and M.S. degrees in electrical engineering from the University of the Philippines at Quezon City, Philippines, in 1968 and 1973, respectively. Starting as an Instructor in Electrical Engineering at the University of the Philippines in 1968, he was an Associate Professor in Electrical Engineering there before commencing his doctoral studies at Northwestern University, Evanston, IL. He received the Ph.D. degree in Electrical Engineering from Northwestern University in 1984.

His interests include microwave-enhanced energy conversion and thermal processes, millimeter-wave technology, and microwave devices.

Morris E. Brodwin (A'49–M'55–SM'68) received the M.S. and Ph.D. degrees from Johns Hopkins University, Baltimore, MD in 1951 and 1957, respectively. While at the university, he pursued studies in applied and theoretical microwave communications and radar. His research area was in the application of ferrites to microwave problems.

In 1958, he joined the faculty of Northwestern University, Evanston, IL, where he is now Professor of Microwave Engineering in the Electrical Engineering and Computer Science Department and is specializing in the fields of microwave characterization and thermal processing.

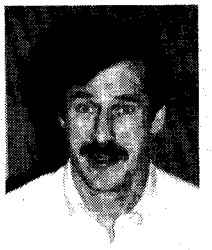

Gregory A. Kriegsmann received the M.S. degree in electrical engineering and the Ph.D. degree in applied mathematics from the University of California at Los Angeles in 1970 and 1974, respectively.

He was a Courant Instructor in Applied Mathematics at New York University, New York, NY, from 1974 to 1976. He is presently an Associate Professor in the Department of Engineering Sciences and Applied Mathematics at Northwestern University, Evanston, IL. His research interests include the development of numerical and asymptpotic methods for solving wave propagation problems.